IEEE Access
Multidisciplinary : Rapid Review : Open Access Journal

Received 24 April 2025, accepted 1 May 2025, date of publication 5 May 2025, date of current version 12 May 2025.

Digital Object Identifier 10.1109/ACCESS.2025.3566985

RESEARCH ARTICLE

Optimized Metamaterials for Design of Enhanced-Performance High Order Mode Dipole-Driven Yagi-Uda Antenna for Millimeter Wave Applications

BASHAR A. F. ESMAIL[1], (Member, IEEE), DUSTIN ISLEIFSON[1], (Senior Member, IEEE), SLAWOMIR KOZIEL[2,3], (Fellow, IEEE), AND ANNA PIETRENKO-DABROWSKA[3], (Senior Member, IEEE)

[1]Department of Electrical and Computer Engineering, University of Manitoba, Winnipeg, MB R3T 5V6, Canada
[2]Department of Engineering, Reykjavik University, 102 Reykjavík, Iceland
[3]Faculty of Electronics, Telecommunications and Informatics, Gdańsk University of Technology, 80-233 Gdańsk, Poland

Corresponding author: Slawomir Koziel (koziel@ru.is)

This work was supported in part by the Icelandic Centre for Research (RANNIS) under Grant 2410297, and in part by the National Science Centre of Poland under Grant 2022/47/B/ST7/00072.

ABSTRACT This paper presents the development of a Yagi antenna optimized for third-order mode operation within the millimeter-wave (mmWave) spectrum. A third-order mode driven dipole, along with a reflector, is introduced to enhance the antenna's gain. The rigorous numerical optimization procedure was employed to precisely adjust the dimensions and positions of the driven dipole, director, and reflectors. The optimized Yagi antenna operates within the fifth generation (5G) band at 28 GHz, with a bandwidth of 2.6 GHz. Radiation pattern analysis indicates that the gain of the antenna in this higher resonant mode exceeds that of a conventional Yagi-Uda antenna, achieving a gain of 9.35 dBi at 28 GHz. To further increase the gain and address the path loss challenges in the mmWave spectrum, a near-zero index metamaterial (NZIM) array was integrated. A 5×5 unit cell array was embedded into the same antenna substrate, positioned in front of the reflector. The metamaterial array was optimized using the trust-region (TR) algorithm, resulting in a significant gain enhancement, reaching 13.8 dBi at 28 GHz while maintaining the operational bandwidth in terms of impedance matching. The antenna was subsequently fabricated and tested, with experimental results demonstrating a strong correlation with the simulated outcomes across all key parameters.

INDEX TERMS Metamaterials, millimeter-wave spectrum, trust-region algorithm, Yagi antenna.

I. INTRODUCTION

Advancements in wireless communications over the past decade have been notable, especially in terms of broadened bandwidth and higher data rates. To meet these requirements by the communication hardware, fifth generation (5G) technology has become a major focus of research. The millimeter-wave (mmWave) band, a key aspect of 5G technology, provides benefits such as low latency, abundant spectrum availability, and gigabit-per-second data speeds. Implementing 5G systems is proposed with allocated frequency bands for mobile networks at 28, 38, 60, and 73 GHz [1], [2], [3]. Many literature reports delve into the frequencies of 28 GHz, highlighting their satisfactory bandwidth and lower path losses in comparison to higher mmWave frequencies [4], [5], [6]. A comprehensive study highlights several challenges in mmWave propagation, including path or transmission loss and shadowing, indicating that antennas

The associate editor coordinating the review of this manuscript and approving it for publication was Olutayo O. Oyerinde.

operating in this band experience significant losses [7]. Consequently, achieving high gain is a primary goal in designing antennas for this band.

In mmWave applications, end-fire antennas such as dipoles and Yagi-Uda structures printed on substrates are widely used [8], [9]. The Yagi-Uda antenna is one of the most popular end-fire antennas, commonly chosen for communication and radar systems due to its simple, low-profile structure, convenient feeding, adequate gain, high radiation efficiency, and low manufacturing cost [10]. Traditional Yagi-Uda antennas usually feature a driven element, a reflector, and directors, with the driven element serving as the core component. Basic-mode dipoles are commonly used as driven elements; however, they offer limited gain. This gain limitation is inherent to conventional Yagi-Uda antennas due to their reliance on a single basic-mode driven dipole. Similarly, other basic-mode driven elements, such as monopoles, loops, patches, and bow-ties, have been explored in [11], [12], [13], [14], but their gain remains restricted to below 6 dBi. To enhance gain, 3D or multilayer-stacked designs are used, though these result in larger sizes and additional losses [15], [16], [17]. Array configurations are a widely adopted technique for enhancing antenna gain [18], [19]. In [18], a 1 × 4 Yagi antenna array was proposed to improve end-fire gain, achieving a peak gain of 11.83 dBi at 20 GHz. Similarly, in [19], a 1 × 8 Yagi slotted array antenna was designed to enhance gain performance, attaining a maximum gain of 11.16 dBi at 28 GHz. However, while these array configurations offer improved gain, they also increase the overall antenna size, add complexity to the design process, and introduce losses due to the intricate feed network. Several directional millimeter-wave antennas with improved performance have been reported in the literature, including helical antennas [20], [21], Vivaldi antennas [22], [23], and leaky-wave antennas [24], [25]. In [20], a moderately tapered helical structure is employed to achieve a wide impedance bandwidth covering 24 to 32 GHz, with a peak gain of 7.8 dBi. In [21], a compact single-turn helix antenna is proposed, offering a bandwidth of 26.25–30.14 GHz and a peak gain of 5.9 dBi. A super wideband Vivaldi antenna covering the frequency range of 22.5–45 GHz has been proposed for 5G millimeter-wave applications [22]. The antenna exhibits a nearly constant end-fire radiation pattern across the band, with a measured gain ranging from 5.5 to 8.5 dBi. The authors of [23] proposed a 1 × 4 Vivaldi antenna array designed to achieve a wide operational bandwidth ranging from 21.63 to 28.81 GHz, with a measured gain varying between 10.5 and 12.5 dBi. In [24] and [25], the authors presented 12-element leaky-wave antenna designs targeting high-performance millimeter-wave applications. The antenna reported in [24] demonstrates a broad operating bandwidth of 28.3–31.8 GHz with a peak gain of 15.5 dBi. Meanwhile, the array proposed in [25] operates over the 56.3–63.4 GHz range and achieves a maximum gain of 13.4 dBi. Although the proposed antennas demonstrate good performance in terms of bandwidth, the gain in most cases is moderate. In some designs, the 3D structure, bulky size, and design complexity present challenges, particularly in the millimeter-wave band.

Modifying the length of the Yagi driven element can enhance both gain and directivity, as this excites a higher-order resonant frequency. In the fundamental mode, the driven element resonates when its length is approximately half the wavelength ($\lambda/2$). Traditional Yagi antenna designs primarily focus on this first resonance [26], while higher-order resonances—occurring at odd multiples of half wavelengths—have received limited attention in the literature. However, recent studies have proposed high-order mode dipole-driven approaches to improve directivity [27], [28]. Incorporating these techniques, along with optimally designed parasitic elements, into the Yagi–Uda antenna structure can significantly enhance gain, which is crucial for mitigating path loss at millimeter-wave frequencies. The third-order mode involves exciting a higher-order current distribution in the driven element rather than relying on the fundamental half-wavelength resonance. In this mode, the current magnitude along the driven element follows a cosine distribution, leading to improved gain and directivity while reinforcing the Yagi antenna's end-fire radiation characteristics.

Alternatively, metamaterials provide a cost-effective means to improve gain without a considerable expansion of the antenna's size [29], [30]. Metamaterials are an extraordinary class of engineered materials with unique properties not found in nature. Incorporating these composite structures into different antennas can greatly enhance their gain performance [31], [32] [33], [34], [35]. The authors of [31] used seven layers of metamaterials, along with six air gaps above a patch antenna, to achieve a gain of 13.6 dBi at 28 GHz. Similarly, in [32], two layers of metamaterials were incorporated in the end-fire direction of a dipole array, increasing the gain to 11.0 dBi at 28.5 GHz. Likewise, in [33], a single layer of different metamaterial structures was added over a slotted patch antenna, resulting in a maximum gain of 12.7 dBi at 28 GHz. In [34], a patch antenna was integrated with a single layer of metamaterial positioned 16 mm above the patch, resulting in an enhanced gain of 11.94 dBi at 28 GHz. However, the inclusion of metamaterial layers adds to the size and complexity of the design, effectively creating a 3D structure. The authors of [35] proposed a two-stage approach to enhance the antenna gain. In the first stage, a non-uniform dipole array was implemented, achieving a gain of 8.1 dBi. In the second stage, a 5 × 7 metamaterial array was incorporated in proximity to the dipole array, further improving the gain to 11.21 dBi. Developing a Yagi-Uda antenna with a third-order mode dipole driver and optimized metamaterials can result in a reliable, high-performance antenna suitable for mmWave applications.

In this study, the high gain Yagi–Uda antenna, using a third-order mode dipole as the driven element with optimized metamaterials, is designed and experimentally validated for mmWave applications. The design undergoes two optimization phases to enhance the performance of both the stand-alone Yagi antenna and the metamaterial-enhanced version. The Yagi antenna, consisting of a third-order mode-driven dipole, reflectors, and a director, is initially optimized using the trust-region (TR) algorithm to meet the target gain and bandwidth requirements. In the second phase of this study, a metamaterial array is integrated onto the same substrate, positioned in front of the director, and optimized to further enhance the antenna's gain. Conducting extensive parametric studies on various components, including the director, driven dipole, reflector, and ground, is both time-consuming and computationally intensive. The complexity is further amplified with the addition of a metamaterial array, making manual parameter adjustments after each simulation impractical and resource-intensive. Moreover, it is necessary to simultaneously handle several objectives (impedance matching and gain enhancement). Traditional means, such as parameter sweeping, are unable to handle such tasks. To overcome this challenge, a rigorous optimization technique was employed to streamline the design process and efficiently achieve optimal performance. The Yagi–Uda antenna, using a third-order-mode dipole as the driven element with optimized metamaterials, is designed and fabricated to enable experimental validation. To the best of our knowledge, no prior studies have explored a compressed third-order Yagi-Uda antenna design incorporating short reflectors for performance enhancement. Furthermore, there are no existing works that combine all the key innovations presented in this study—namely, the compressed third-order Yagi structure, a dual-stage optimization framework, and near-zero-index (NZI) metamaterial enhancement—within a single antenna system. Although certain components of this methodology have been investigated individually in previous studies, their combined implementation—as proposed in this work—yields improved performance and practical feasibility not previously documented in the literature. The key technical contributions and originality of this work can be summarized as follows:

I. Development of a compact, low-profile Yagi–Uda antenna that leverages a compressed third-order mode dipole as the primary driven element. The design integrates parasitic reflectors alongside a truncated ground to enhance end-fire radiation characteristics. This configuration enables the antenna to achieve a high peak gain of 9.35 dBi at 28 GHz, while maintaining a wide impedance bandwidth of 2.6 GHz, making it well-suited for millimeter-wave applications.

II. Recognizing the challenges and inefficiencies associated with parametric sweeping in high-dimensional, nonlinear Yagi antenna design spaces, this work employs a rigorous gradient-based optimization technique as the first stage. The proposed method enables the precise formulation of performance objectives and constraints, ensuring efficient convergence toward optimal solutions that balance high gain, wide bandwidth, and structural requirements.

III. Design and integrate a metamaterial with a broad near-zero index (NZI) response within the 27–29 GHz frequency range into a Yagi antenna, enhancing its gain to a peak value of 13.8 dBi at 28 GHz, while maintaining a compact and efficient geometry.

IV. Implementing and incorporating a second stage of rigorous numerical optimization framework to enhance the metamaterial antenna performance concerning its gain and reflection response. The key component in both optimization stages is a dedicated formulation of the merit function incorporating regularization mechanism to effectively control the primary objective (e.g., gain) and constraints (e.g., impedance matching conditions).

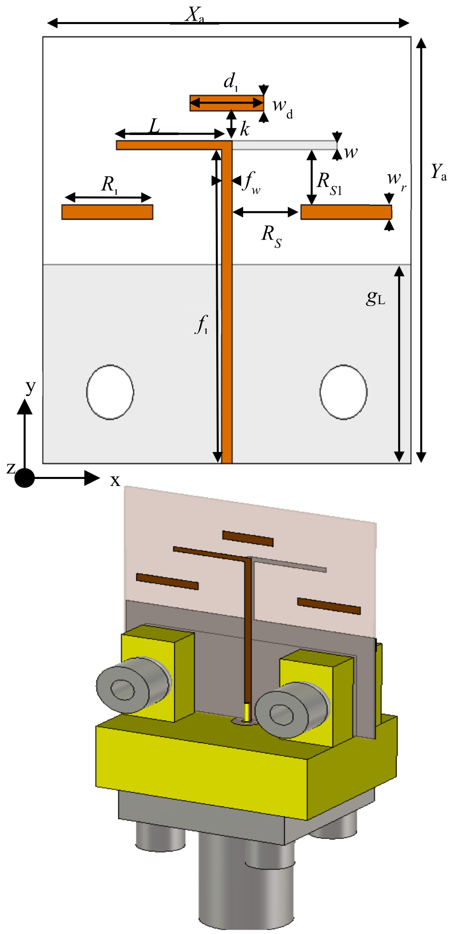

FIGURE 1. The configuration of the Yagi antenna, dimensions; $X_a = 15$, $Y_a = 17$, $L = 4.189$, $w = 0.293$, $d_1 = 2.058$, $w_d = 0.828$, $R_1 = 2.705$, $w_r = 0.828$, $R_S = 3.143$, $R_{S1} = 1.9$, $f_W = 0.388$, $f_1 = 11.346$, and $g_L = 6.522$, $k = 0.649$. All dimensions are in mm.

II. HIGHER ORDER MODE YAGI-UDA ANTENNA

The configuration of the proposed Yagi antenna is illustrated in Fig. 1. It consists of a third-order mode dipole-driven element, two short reflectors, a director, and truncated ground.

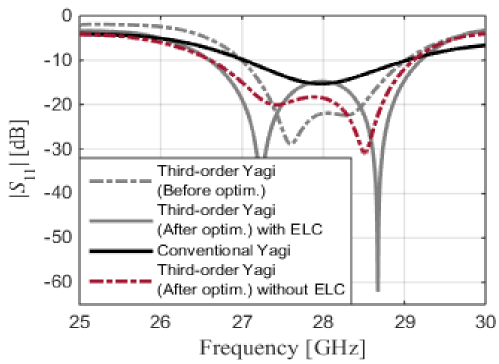

FIGURE 2. Reflection coefficients of the conventional Yagi and third-order Yagi before and after optimization.

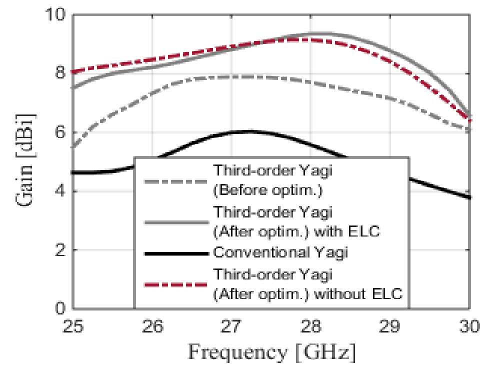

FIGURE 3. Gain plots of the conventional Yagi and third-order Yagi before and after optimization.

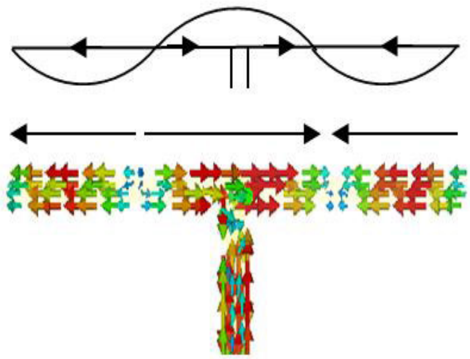

FIGURE 4. Surface current of the dipole driven element at 28 GHz.

It is printed on Rogers RO3010 with a dielectric constant of 10.2, tangent loss of 0.0035, and thickness of 0.254 mm. The director and two reflectors are printed on the front side of the substrate. The reflectors are chosen for best gain performance and are located parallel to and beneath the driven element along the y-axis. The use of shorter reflectors is advantageous for microstrip line feeding, as the traditional method of using a coaxial connector is inherently limited by narrow bandwidth constraints. The initial design phase involved a comprehensive evaluation of the reflector placement, during which the reflectors were positioned above the driven element, adjacent to the director. However, this configuration caused the antenna's directivity to shift predominantly toward the negative y-axis. This undesired behavior was attributed to the reflectors redirecting the radiated energy in the opposite direction of the intended end-fire axis. Consequently, this arrangement led to a noticeable reduction in gain along the end-fire (y) direction, undermining the primary performance objective of the design. To address these issues, the reflector was repositioned beneath the driven element to improve overall performance. The positions and dimensions of the reflectors were meticulously adjusted through formal optimization to achieve the best possible performance in terms of gain and bandwidth. The two reflectors on the x-axis work as a complete reflector. The director, which is an essential part of the Yagi antenna, is placed parallel to, and above, the drive element along the y-axis. The dimensions of this part were also carefully adjusted during the optimization stage as it has an essential role in enhancing the antenna directivity.

The third-order mode dipole typically has a length of $3\lambda/2$ (where λ represents the wavelength at a frequency of 28 GHz). However, practical implementations often seek to reduce the physical size of higher-order mode antennas while maintaining their resonant properties. To achieve this, the compressed third-order mode is employed, utilizing a length of $3\lambda/4$ instead of $3\lambda/2$ [27]. This approach enables the design of a more compact and efficient driven dipole while preserving its desired electromagnetic performance. Figure 2 illustrates the reflection coefficients of both the conventional Yagi and the third-order Yagi before and after optimization. For comparison, a Yagi antenna operating in the basic mode ($\lambda/2$) is presented, offering a bandwidth range of 27–29 GHz. In contrast, the third-order mode Yagi-Uda antenna exhibits enhanced bandwidth performance in both configurations—with and without the End Launch Connector (ELC). The design without the ELC shows a slightly narrower impedance bandwidth of 2.5 GHz (26.6–29.1 GHz), compared to 2.6 GHz (26.6–29.2 GHz) when the ELC is included. Nevertheless, the proposed antenna demonstrates superior reflection characteristics in both cases compared to the conventional Yagi-Uda design. Figure 3 illustrates the gain characteristics of both designs. The conventional Yagi antenna achieves a maximum gain of 6 dBi within the operating frequency band. In comparison, the proposed third-order mode Yagi-Uda antenna demonstrates a consistently higher gain across the entire band, both with and without the ELC. Specifically, the design incorporating the ELC attains a peak gain of 9.35 dBi at 28 GHz, while the version without the ELC achieves 9.15 dBi. This indicates a gain improvement of 0.2 dBi attributable to the presence of the ELC. Figure 4 illustrates the current distribution of the antenna's driven dipole at the target frequency of 28 GHz. The dipole exhibits reverse currents compared to basic mode. The sinusoidal current distribution along the dipole verifies that it is functioning in its third resonant mode. The ELC was incorporated into the simulation model to accurately replicate the conditions of

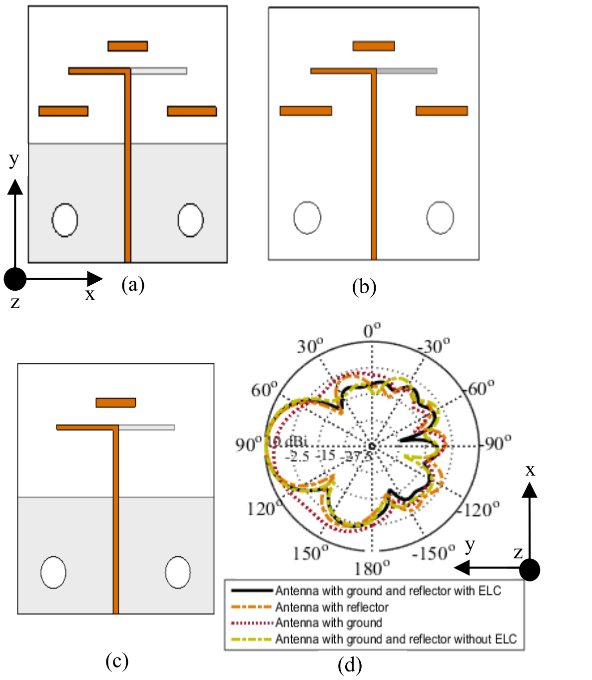

FIGURE 5. **Yagi antenna configurations: (a) with both reflectors and truncated ground, (b) with reflectors only, (c) with truncated ground only, and (d) the radiation pattern for the three cases.**

the practical measurement environment and ensure a closer correlation between simulated and measured results.

III. YAGI PERFORMANCE OPTIMIZATION

The Yagi antenna underwent initial optimization as a separate structure, concentrating on enhancing its gain performance (i.e., increasing the maximum gain). This process is driven by adjusting specific parameters $x = [L\ w\ d_1\ w_d\ R_1\ w_r,\ R_{s1}\ f_w\ f_1\ g_L]^T$, all illustrated in Fig. 1. The following ranges delineate the search space X : $4 \leq L \leq 5.8$ mm, $0.3 \leq w \leq 0.6$ mm, $2 \leq d_1 \leq 6$ mm, $0.3 \leq w_d \leq 0.8$ mm, $1 \leq R_1 \leq 4.5$ mm, $0.3 \leq w_r \leq 0.7$ mm, $0.4 \leq R_s \leq 3$ mm, $0.2 \leq f_w \leq 0.6$ mm, $10 \leq f_1 \leq 12$ mm, $6 \leq g_L \leq 9$ mm. Moreover, the optimization process is subject to the following geometric constraints: $R_1 + R_s < X_a/2$ and $f_1 + k + w_d < Y_a$, which are introduced to ensure geometrical consistency of the antenna. The primary objective was to maximize the gain $|G(x_i f_0)|$ at $f_0 = 28$GHz, and to ensure $|S_{11}(x_v f)| \leq -10$ dB within the frequency range $f \in F = [26.6\ 29.2]$ GHz. Considering the primary aim and the constraints, the cost function to be minimized was defined as follows

$$U(\boldsymbol{x}) = -G(\boldsymbol{x}) + \beta\left[\frac{\max\{S(x) + 10, 0\}}{10}\right]^2 \tag{1}$$

where

$$G(\boldsymbol{x}) = G(\boldsymbol{x}, f_0) \tag{2}$$

and

$$S(\boldsymbol{x}) = \max_{f \in F}\{|S_{11}(\boldsymbol{x}, f)|\} \tag{3}$$

are the gain at the center frequency and maximum in-band reflection, respectively. The optimum design $\boldsymbol{x}^*$ is found by solving

$$\boldsymbol{x}^* = \arg\min_{\boldsymbol{x} \in X} U(\boldsymbol{x}) \tag{4}$$

It is important to note that minimizing the objective function U enhances the gain at $f_0 = 28$GHz and enforces the matching condition over the entire bandwidth of interest F. The penalty coefficient β [30] was set to 100 to ensure that $|S_{11}(\boldsymbol{x}, f)| \leq -10$ dB across the bandwidth F, with a tolerance within a fraction of a decibel. The reflection requirement is technically an inequality constraint, but because it requires costly EM analysis to evaluate, implicit handling is more efficient [36]. The TR gradient-based algorithm [37] was used to solve problem (4), with antenna response sensitivities estimated by means of finite differentiation [38]. The TR algorithm produces a sequence of approximations $\boldsymbol{x}^{(i)}$, $i = 0, 1, \ldots$, to the optimal solution $\boldsymbol{x}^*$, with each update $\boldsymbol{x}^{(i+1)} = \text{argmin}\left\{\boldsymbol{x};\ \left\|\boldsymbol{x} - \boldsymbol{x}^{(i)}\right\| \leq d^{(i)}:\ U_L(x)\right\}$. The local objective function U_L is defined as in (1) but is evaluated using a first-order Taylor expansion model of the antenna characteristics, rather than relying on direct EM analysis. The search region size $d^{(i)}$ was adaptively adjusted according to standard TR rules [36]. The TR subproblem was solved using the SQP algorithm implemented in Matlab Optimization Toolbox [39]. The termination criterion is based on convergence in the solution, specifically when $\left(\left\|x^{(i+1)} - x^{(i)}\right\| < \varepsilon\right.$, here, $\left.\varepsilon = 10^{-3}\right)$. For the convenience of the reader, below, we summarize the operating steps of the TR algorithm:

1. Problem formulation: Solve $x^* = \text{argmin}\ \{x \in X : U(x)\}$ (cf. (4)), with $x^{(0)}$ being an initial design;
2. Algorithm operation: Generate a series $x(i)$, $i = 0, 1, \ldots$, of approximations to x^*. The new (candidate) vector $x(i+1)$ is obtained by solving

$$\boldsymbol{x}^{(i+1)} = \arg\min_{\|\boldsymbol{x} - \boldsymbol{x}^{(i)}\| \leq d^{(i)}} U_L(\boldsymbol{x}) \tag{5}$$

where

$$S_{11.L}^{(i)}(\boldsymbol{x}, f) = S_{11}(\boldsymbol{x}^{(i)}, f) + \nabla S_{11}(\boldsymbol{x}^{(i)}) \cdot (\boldsymbol{x} - \boldsymbol{x}^{(i)}) \tag{6}$$

$$G_L^{(i)}(\boldsymbol{x}, f) = G(\boldsymbol{x}^{(i)}, f) + \nabla G(\boldsymbol{x}^{(i)}) \cdot (\boldsymbol{x} - \boldsymbol{x}^{(i)}) \tag{7}$$

are first-order Taylor expansion of the high-resolution the reflection and gain responses, respectively at $\boldsymbol{x}^{(i)}$. The gradients ∇S_{11} and ∇G are estimated using finite differentiation (FD) [38], which incurs additional n EM analyzes of the antenna.
3. Objective function: The function UL is identical to the function U of (3), but it is computed based on the first-order linear expansion models of antenna characteristics.

4. Gain ratio r: EM-evaluated versus linear-model predicted objective function improvement

$$r = \frac{U(\boldsymbol{x}^{(i+1)}) - U(\boldsymbol{x}^{(i)})}{U_L(\boldsymbol{x}^{(i+1)}) - U_L(\boldsymbol{x}^{(i)})} \tag{8}$$

35. Trust region size $d^{(i)} > 0$: Adaptively adjusted based on r; $d^{(i+1)} = d^{(i)} m_{incr}$ if $r > r_{incr}$, and $d^{(i+1)} = d^{(i)}/m_{decr}$ if $r < r_{decr}$; standard control parameter values are $r_{incr} = 0.75$, $r_{decr} = 0.25$, $m_{incr} = 1.5$, $m_{\mathrm{decr}} = 2$ [37].
6. Acceptance of the new iteration point: $\boldsymbol{x}^{(i+1)}$ is accepted only if $r > 0$ (i.e., EM-evaluated objective function has been improved); otherwise, the iteration is repeated with the reduced TR size;
7. Algorithm termination: Convergence in argument $\left(\left\|x^{(i+1)} - \boldsymbol{x}^{(i)}\right\| < \varepsilon\right)$ or sufficient reduction of the TR size ($d^{(2)} \leq \varepsilon$); the termination threshold is set to $\varepsilon = 10^{-3}$.

The algorithm is provably convergent to the local minimum of the cost function $U(\boldsymbol{x})$ under mild assumptions concerning the smoothness of the functions involved (they must be at least continuously differentiable [37]). Although this condition is not necessarily fulfilled for EM-simulated characteristics, the algorithm is also convergent due to eventual reduction of the TR size. The initial design $\boldsymbol{x} = [4.30\ 0.30\ 3.00\ 0.55\ 3.70\ 0.503.00\ 0.30\ 116.0]^T$ was found using parametric studies. The optimized design obtained through optimization was $\boldsymbol{x} = [4.189\ 0.293\ 2.058\ 0.828\ 2.705\ 0.8283.143\ 0.388\ 11.3466.522]^T$ mm. The initial and optimized antenna reflection coefficient and gain are presented in Figs. 2 and 3, respectively. The ELC was included in the optimization process to ensure greater accuracy and consistency between simulation and measurement results. Three parameters had been incorporated into the optimization process to determine the optimal location of the reflectors, which contributed to improving antenna performance. These parameters include: R_1 and w_r, which define the length and width of each reflector; R_s, representing the separation distance between the reflectors and the feed line. These, along with other antenna parameters, were optimized to enhance both bandwidth and gain. As a result, the bandwidth increased from 2 GHz to 2.6 GHz, cf. Fig. 2, and the gain improved from 7.6 dBi to 9.35 dBi, cf. Fig. 3. Three designs of the Yagi antenna are shown in Fig. 5(a), (b), and (c) to evaluate the impact of the reflector and ground on antenna performance. The design in Fig. 5(a) is the proposed configuration, combining the benefits of both the reflector and ground to achieve improved reflection. In Fig. 5(c), the truncated ground plane acts as a reflector, serving as a partially cut-away ground structure that enhances radiation efficiency by redirecting energy toward the end-fire direction (y-direction). Figure 5(d) illustrates the E-plane radiation patterns for the three antenna configurations. The results show that the truncated ground plane effectively reduces back lobe radiation, while the reflector-based design provides higher gain. Furthermore, the radiation patterns of the Yagi-Uda antenna, with both

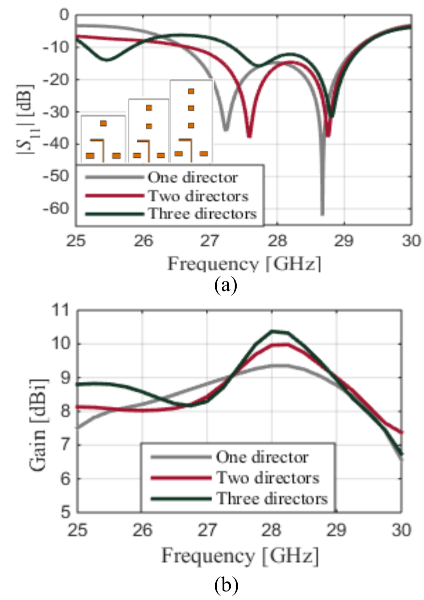

FIGURE 6. The antenna performance with an increasing number of directors: (a) the reflection coefficients and (b) the gain.

reflector and ground plane configurations and with or without ELC, display nearly identical characteristics. This indicates that the presence of the ELC has a minimal effect on the antenna's radiation performance. A comprehensive analysis of the impact of increasing the number of directors on the optimized antenna's performance has been conducted, with the results presented in Fig. 6. The findings reveal that the antenna gain improves to 10 dBi and 10.4 dBi when the number of directors is increased to two and three, respectively. However, while this modification enhances gain, it also leads to an increase in antenna size without significantly improving overall performance. Furthermore, a decrease in gain is observed around 27 GHz when the number of directors is increased from one to three. Additionally, increasing the number of directors results in a reduction in broadband operation, further highlighting the trade-offs associated with this design modification.

IV. METAMATERIAL ANTENNA

Although the Yagi antenna gain is enhanced by using a third-order mode-driven dipole and reflectors, path loss at millimeter waves is dominant, so further improvement in gain is required to ensure signal quality. A set of metamaterial unit cells was embedded on the antenna substrate in front of the director (in the xy-plane). Figure 7 depicts the Yagi antenna with the metamaterial array. A 4×5 array of unit cells was integrated into the same antenna substrate, positioned in front of the director. Simulations were employed to optimize the number of metamaterial unit cells, striking a balance between high gain, bandwidth, and a compact design. To meet the desired gain while maintaining a manageable physical size, the number of metamaterial rows along the y-axis was increased. By incorporating unit cells directly

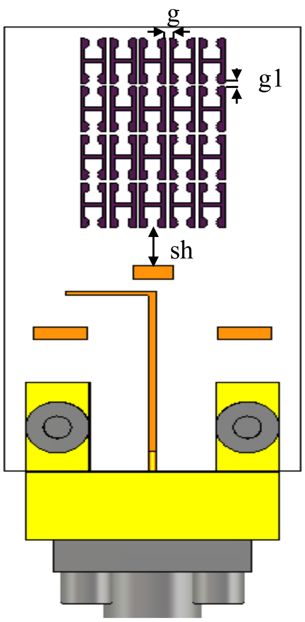

FIGURE 7. The proposed Yagi antenna with a metamaterial array.

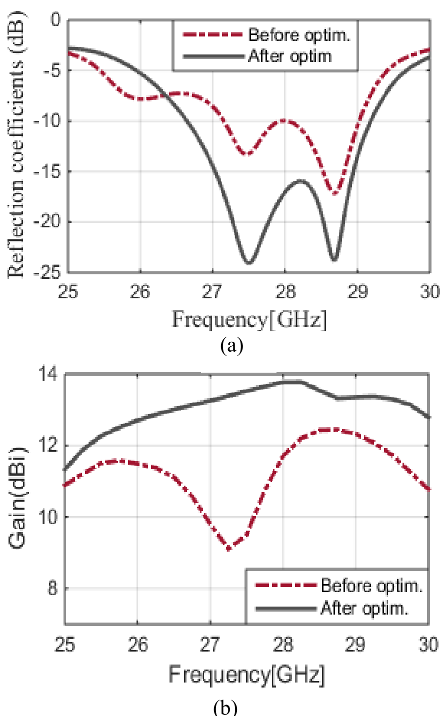

FIGURE 8. Metamaterial antenna performance before and after optimization: (a) Reflection coefficient, and (b) gain.

into the antenna substrate and optimizing their geometric parameters through numerical methods, the design process can be streamlined, minimizing the need for iterative adjustments to geometry dimensions while achieving an optimal design. This approach, which focuses on optimizing the metamaterial within the antenna system itself—rather than designing the metamaterial independently and integrating it

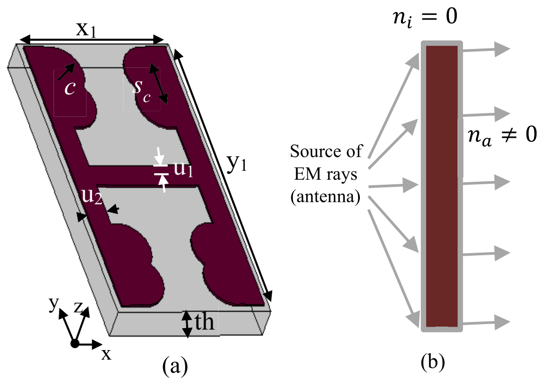

FIGURE 9. (a) Metamaterial configuration. (The dimensions are: x1 = 1.390 mm, y1 = 2.820 mm, c= 0.200 mm, sc= 0.204 mm, u1= 0.103 mm, u2= 0.203 mm, th= 0.254mm), and (b) Gain enhancement mechanism.

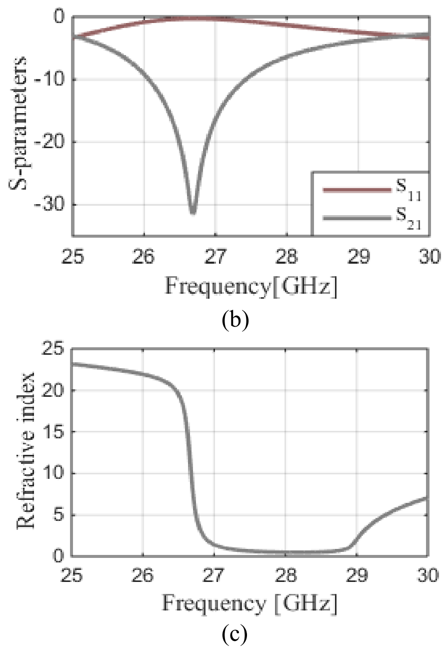

FIGURE 10. Metamaterial performance: (a) S-parameters, and (b) Refractive index.

later—eliminates the need for re-adjusting the number and placement of unit cells, resulting in significant savings in both time and resources compared to handling these tasks separately. In Figs. 8(a) and (b), the reflection coefficient and gain of the Yagi antenna with metamaterial loading are presented, comparing the results before and after optimization. The addition of the metamaterial array impacted the impedance matching performance of the antenna compared to the unloaded version, as shown in Fig. 8(a) and Fig. 2. However, after optimization, the impedance bandwidth improved, becoming nearly identical to that of the unloaded antenna. The metamaterial antenna initially shows a considerable gain increase, reaching 11.8 dBi at 28 GHz, cf. Fig. 8(b). This highlights the potential for numerical optimization

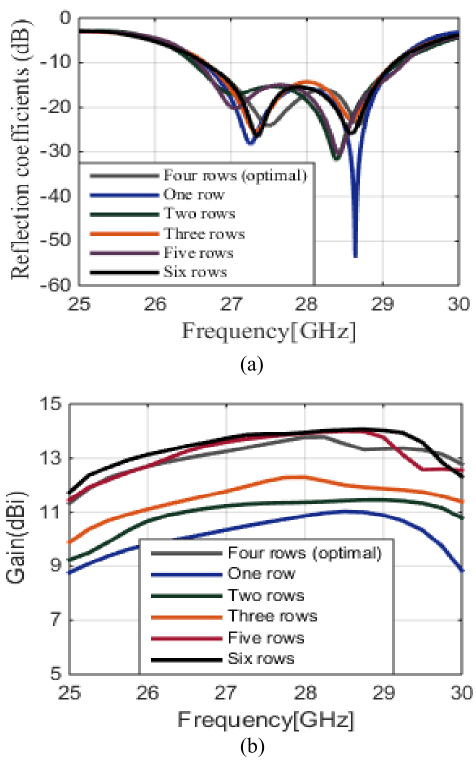

FIGURE 11. Performance of the metamaterial antenna with varying numbers of array rows: (a) reflection coefficient and (b) gain.

techniques to push performance even further. Through the application of the TR algorithm, the unit cell dimensions were fine-tuned, leading to a gain boost to 13.8 dBi at 28 GHz, as depicted in Fig. 8(b). The steps involved in the optimization are discussed in Section V.

V. GAIN PERFORMANCE OPTIMIZATION

The second stage of the optimization process aims to improve the gain of the metamaterial-inspired antenna shown in Fig. 6. This involves refining crucial design parameters of the metamaterials, which are represented by a set of nineteen variables organized into a vector, $x = [x_1\ y_1\ g\ g_1\ c\ sh\ u_1\ u_2\ s_c\ L\ w\ d_1 w_d\ R_1\ w_r\ R_s f_w f_1\ g_L]^T$. Some of these parameters pertain specifically to the metamaterial, such as g and g_1, which represent the gaps between the unit cells along the x- and y-axes, respectively, cf. Fig. 6. Additionally, sh represents the distance between the director and the metamaterial array. The remaining ten parameters are related to the Yagi antenna structure and were utilized in the second optimization phase to provide additional flexibility in enhancing both bandwidth and gain. The parameter space X is defined as the interval $[L_o, u_p]$, where the lower and upper bound vectors are given by $L_o = [1.0\ 1.4\ 0.2\ 0.2\ 0.15\ 0.2\ 0.1\ 0.2\ 0.2\ 4.0\ 0.3\ 2\ 0.3\ 1.0\ 0.3\ 0.4\ 0.2\ 10\ 6.0]^T$ and $u_p = [2.5\ 3.0\ 0.50\ 0.50\ 0.30\ 1.00\ 0.30\ 0.30\ 0.30\ 5.8\ 0.6\ 6.0\ 0.8\ 4.5\ 0.7\ 3.0\ 0.6\ 12\ 9.0]^T$, with all values in millimeters. Additional constraints were applied to guarantee the geometric consistency of the metamaterial: $f_1 + k + w_d + sh + 4y_1 + 3g_1 < 28$ mm, $5x_1 + 4g < X_a$, and $4c - x_1 < -0.2$mm. The initial design $x = [1.40\ 2.40\ 0.20\ 0.20\ 0.15\ 0.20\ 0.10\ 0.20\ 0.20\ 4.18\ 0.29\ 2.05\ 0.82\ 2.70\ 0.82\ 3.14\ 0.38\ 11.34\ 6.52]^T$ was obtained from parametric studies, except for the last ten parameters, which were retained from the initial optimization phase. The final design $x = [1.390\ 2.820\ 0.200\ 0.202\ 0.200\ 2.370\ 0.103\ 0.203\ 0.204\ 4.18\ 0.29\ 2.00\ 0.89\ 2.74\ 0.77\ 3.26\ 0.423\ 11.20\ 6.70]^T$, was obtained using the algorithm described in Section III, requiring less than one hundred EM antenna simulations. The gain has noticeably improved through the use of the metamaterial array and the second optimization phase, as observed in Fig. 8(b). The final design achieves an average gain of approximately 12.8 dBi, with a maximum of 13.8 dBi at 28 GHz, while the reflection constraint is maintained similarly to that of a standalone antenna, cf. Fig. 8 and Fig. 2. Figure 9 illustrates the configuration of the proposed metamaterial, which is designed on the same Rogers RO3010 substrate as the antenna to ensure seamless and compatible integration. This metamaterial is intended to improve the gain across the entire operating band. Figure 9(a) displays the simulated model, printed on the front of the substrate, with its dimensions detailed in the figure caption. Given that the incident wave from the Yagi antenna propagates in the y-direction, cf. Fig. 1, the two ports of the unit cell were positioned accordingly. The waveguide surfaces along the x-direction were defined as perfect electric conductors (PEC), while the surfaces along the z-direction were defined as perfect magnetic conductors (PMC). The unit cell S-parameters and the refractive index are depicted in Fig. 10. The unit cell exhibits a near zero refractive index (NZIM) across the desired band. The NZIM functions as a meta-lens, concentrating radiation in the desired end-fire direction. When combined with antennas, this unique characteristic, the NZIM, can lead to significant gain improvement. The mechanism behind gain enhancement can be understood through Snell's law of refraction, given by $\boldsymbol{sin\alpha_i} \cdot n_i = \boldsymbol{sin\alpha_a} \cdot n_a$, where $n_i(\alpha_i)$ and $n_a(\alpha_a)$ represent the refractive indices (angles) of the metamaterial and air, respectively. Figure 9(b) illustrates that when incident rays move from a medium with a near zero refractive index ($n_i = n_m. \approx 0$) into air ($n_{air} = 1$), the refracted rays spread out perpendicular to the interface. Consequently, the phase change in the electromagnetic wave becomes negligible, resulting in gain enhancement in the end-fire direction. The impact of increasing the number of metamaterial array rows was investigated, and the results are presented in Fig. 11. A comprehensive analysis was conducted to determine the optimal array configuration, ensuring a balanced trade-off between gain enhancement, bandwidth, and compactness. During the selection process, the number of rows was varied from 1 to 6, while maintaining the original antenna parameters unchanged. As shown in Fig. 11, increasing the number of rows resulted in a progressive gain improvement, reaching a peak value of 13.8 dBi with the 4 × 5 configuration. However, further expansion of the array beyond this configuration led to only marginal

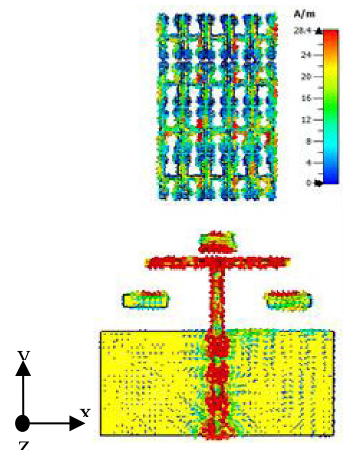

FIGURE 12. Surface current distribution of the metamaterial antenna at 28 GHz.

gain improvements while significantly increasing the overall antenna profile. Additionally, the variation in the number of array rows had minimal impact on the reflection coefficient, as the antenna continued to cover nearly the same frequency band as the standalone configuration. Based on these findings, the 4 × 5 configuration was identified as the most efficient choice for achieving optimal performance while maintaining a compact design. The surface current distribution for the proposed metamaterial-based antenna, presented in Fig. 12, demonstrates the metamaterial's ability to influence EM wave behavior. The metamaterial array functions as an efficient guiding medium, concentrating radiated energy along the end-fire direction (aligned with the y-axis). This focused propagation contributes to an enhancement in antenna gain performance.

A few comments should be made concerning the specific arrangement of the optimization process, selection of optimization parameters, and constraints. The design task has been split into two parts. The first stage only included the core antenna parameters, which were selected as those having main effect on antenna responses. In the second stage, the parameters describing the metamaterial array were incorporated as well to achieve extra gain boost. At this stage, the core antenna parameters are also used to increase the number of degrees of freedom. This arrangement allows for facilitating identification of the maximum gain, which would be more difficult if a one-stage approach was used (a gain-improved design found in the first stage where less parameters were tuned provides a better starting point for the second stage). The constraint selection is rooted in two conditions: (i) the need to preserve impedance matching bandwidth, (ii) the need to preserve geometrical consistency of the antenna. The first constraint is handled implicitly by adding an appropriate penalty term (cf. (1)), which is because it is a computationally heavy condition (each evaluation of it required a separate EM simulation). As indicated in [32], implicit handling is more efficient for computationally expensive constraints. The geometrical constraints are fulfilled by

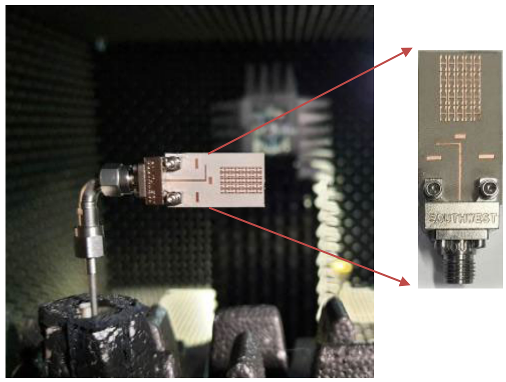

FIGURE 13. Yagi antenna setup in the anechoic chamber, with the inset displaying a close-up of the fabricated prototype.

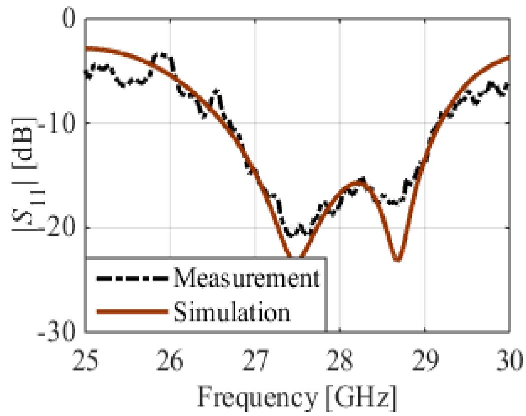

FIGURE 14. Comparison of simulated and measured reflection coefficients.

assigning appropriate lower and upper bounds for design parameters, which ensure that the building blocks of the antenna and the metamaterial array do not overlap, or do not extend beyond the substrate area. On the other hand, they ensure that the fabrication constraints are met as well (the minimum size of any detail cannot be smaller than 0.2 mm for the technological process used to manufacture the antenna, here, LPKF protolaser). Finally, we chose a local optimization algorithm because it is the only practical option to due high computational cost of antenna simulation. None of the global search techniques can be employed because of prohibitive CPU expenses. Nature-inspired methods such as genetic algorithms or particle swarm optimizers are particularly unsuitable due to their dramatically poor cost effectiveness. Furthermore, preliminary studies (including geometry evolution and parameter sweeping) provide us with reasonably good starting point, making local optimization sufficient to find the maximum gain.

VI. ANTENNA FABRICATION AND PERFORMANCE MEASUREMENT

To validate the simulation results and showcase its potential for 5G mmWave applications, the metamaterial-based Yagi

TABLE 1. Benchmarking the proposed metamaterial antenna against current state-of-the-art designs.

Ref.	Antenna (Size (λ))	Frequency (GHz)	Bandwidth(GHz) (Fractional(%))	Max. Gain dBi	Mechanism (structure)
[18]	Yagi antenna (4.67×2.07×0.15)	20	16.51–21 (22.4)	11.83	1×4 Yagi array
[19]	Yagi antenna (3.2×2.62×0.21)	28	26.79-28.38 (5.6)	11.16	1×8 Yagi array
[20]	Helix Antenna (2.86×1.03×0.14)	28	24–32 (28.5)	7.8	Double-helix antenna
[21]	Helix Antenna (1.40×1.03×0.0189)	28	26.25–30.14 (13.8)	5.9	Single turn helix
[23]	Vivaldi Antenna (5.14× 3.73 × 0.047)	28	21.63–28.81 (28.4)	12.5	1 × 4 Vivaldi array
[24]	Leaky wave antenna (8.2×6×3.5)	30	28.3–31.8 (11.6)	15.5	12-element leaky wave antenna
[25]	Leaky wave antenna (6.48 × 4× 0.144)	60	56.3–63.4 (11.8)	13.4	12-element leaky wave antenna
[31]	Patch antenna (2.60×1.37×0.65)	28	27.2-29 (6.4)	13.67	Seven metamaterial layers (3D)
[32]	Dipole antenna (2.71×1.42×2.92)	28.5	25.6–31.8 (21.7)	11.0	Two metamaterial layer (3D)
[33]	Slotted-patch antenna (2.13×1.20×0.68)	28	25-31 (21.4)	12.7	One metamaterial layer (3D)
[34]	Patch antenna (2.06×1.68×1.50)	28	26.58-29.31 (9.7)	11.94	One metamaterial layer (3D)
[35]	Dipole antenna (4.06×1.27×0.026)	38	23.1- 44.8 (57.1)	8.1	Dipole array
	Metamaterial antenna(4.37×1.37×0.028)	41	23.1- 44.8 (52.9)	11.21	Etching the metamaterials on the substrate (2D)
This work	Yagi antenna (1.59×1.40×0.024)	28	26.6-29.3 (9.7)	9.35	Third-order mode-driven dipole +reflectors (2D)
	Metamaterial antenna(2.61×1.40×0.024)	28	26.6-29.3 (9.7)	13.8	Etching the metamaterials on the substrate (2D)

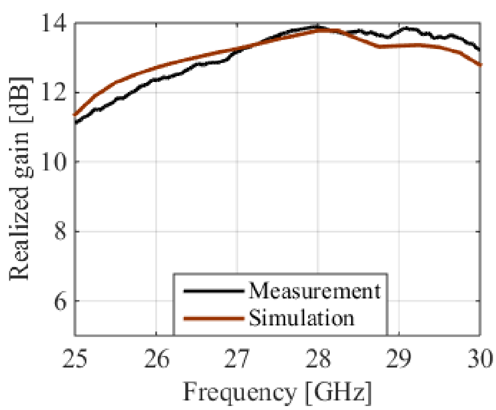

FIGURE 15. Comparison of simulated and measured gains.

antenna, refined through a formal numerical optimization method, was manufactured. The inset of Fig. 13 displays the fabricated prototype. Testing of the antenna's reflection coefficient was performed using an Anritsu vector network analyzer MS4644B, and the radiation patterns were verified inside an anechoic chamber, as shown in Fig. 13. Figure 14 shows a comparison of the simulated and measured reflection coefficients. The antenna demonstrates a simulated wide impedance bandwidth ranging from 26.6 GHz to 29.2 GHz, effectively covering the 5G band at 28 GHz. The $|S_{11}|$ results show excellent agreement between the simulated and measured data, with both covering approximately the same bandwidth. A small discrepancy in the resonance magnitude between the measured and simulated data can be observed, likely due to factors such as fabrication tolerances, cable losses, and assembly errors. Figure 15 presents the realized gain plots of the metamaterial-based Yagi antenna, comparing simulated and measured results. The simulated gain varies from 13 dBi to 13.8 dBi across the operating band. The measured gain is largely in agreement with the simulation results, with some minor deviations, likely caused by previously mentioned issues like inaccuracies in fabrication, assembly, or angular positioning during testing. The co- and cross-polarization radiation patterns of the newly developed antenna are illustrated in Fig. 16 for the E- and H-planes at 28 GHz. The metamaterial antenna exhibits directional radiation patterns in both the E- and H-planes, with minimal cross-polarized field levels, maintaining a low level below −27 dBi. This performance indicates good beam focusing and reduced interference from undesired directions. Additionally, the measured results align closely with the numerical simulations, confirming the accuracy of the design and the

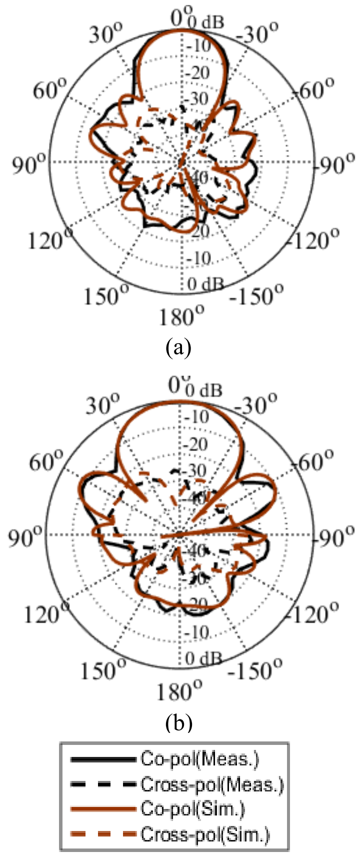

FIGURE 16. Co- and cross-polarization radiation patterns at 28 GHz (a) E-plane and (b) H-plane.

effectiveness of the metamaterial structure in enhancing directional radiation characteristics. The proposed metamaterial antenna has been compared with state-of-the-art designs recently reported in the literature, all of which operate in comparable frequency ranges. The data are summarized in Table 1. In contrast to these designs, the antenna developed here offers high gain, alongside a compact, low-profile structure and wide bandwidth. Additionally, its geometry is simple, making it easy to manufacture using standard PCB techniques.

VII. CONCLUSION

A Yagi-Uda antenna with broadband and high-gain capabilities, incorporating a third-order mode driven dipole and metamaterials, was introduced to cover the 5G frequency range of 27.5–28.35 GHz. The design underwent two optimization phases to enhance the performance of both the stand-alone Yagi and metamaterial antenna. The Yagi antenna, comprising a third-order mode driven dipole, reflectors, and a director, had its component dimensions and locations precisely optimized using the TR algorithm to achieve target gain and bandwidth specifications. The resulting design offers a broad 2.6 GHz bandwidth and a gain of 9.36 dBi at 28GHz, outperforming conventional Yagi designs. In the second stage, an optimization of the metamaterial unit cells' dimensions and spacing was performed using the TR algorithm, yielding a gain increase to 13.8 dBi, while maintaining the standalone Yagi bandwidth. The developed antenna was validated experimentally, showing excellent consistency between simulated and measured outcomes. This design stands out in comparison to recent advancements in the literature, providing a simplified, low-profile system while achieving high gain and wide bandwidth.

REFERENCES

[1] W. Hong, Z. H. Jiang, C. Yu, D. Hou, H. Wang, C. Guo, Y. Hu, L. Kuai, Y. Yu, Z. Jiang, Z. Chen, J. Chen, Z. Yu, J. Zhai, N. Zhang, L. Tian, F. Wu, G. Yang, Z.-C. Hao, and J. Y. Zhou, "The role of millimeter-wave technologies in 5G/6G wireless communications," *IEEE J. Microw.*, vol. 1, no. 1, pp. 101–122, Jan. 2021.

[2] I.-J. Hwang, J.-I. Oh, H.-W. Jo, K.-S. Kim, J.-W. Yu, and D.-J. Lee, "28 GHz and 38 GHz dual-band vertically stacked dipole antennas on flexible liquid crystal polymer substrates for millimeter-wave 5G cellular handsets," *IEEE Trans. Antennas Propag.*, vol. 70, no. 5, pp. 3223–3236, May 2022.

[3] J. Feng, Y. Liang, X. Niu, L. Lu, X. Chen, D. Cheng, Q. Chen, L. Luo, X. Wu, X. Fan, and L. Li, "A compact low-loss high-reliability antenna T/R switch embedded in power combiner for 60-GHz fully differential PA and LNA," *IEEE Microw. Wireless Technol. Lett.*, vol. 35, no. 1, pp. 39–42, Jan. 2025.

[4] A. Muhammad, M. U. Khan, R. S. Malfajani, M. S. Sharawi, and M. Alathbah, "An integrated DRA-based large frequency ratio antenna system consisting of a mm-Wave array and a MIMO antenna for 5G applications," *IEEE Open J. Antennas Propag.*, vol. 5, pp. 368–378, 2024.

[5] J. Ran, C. Jin, P. Zhang, W. Wang, and Y. Wu, "High-gain and low-loss dual-polarized antenna array with reduced sidelobe level based on gap waveguide at 28 GHz," *IEEE Antennas Wireless Propag. Lett.*, vol. 21, pp. 1022–1026, 2022.

[6] B. A. F. Esmail and S. Koziel, "Design and optimization of metamaterial-based dual-band 28/38 GHz 5G MIMO antenna with modified ground for isolation and bandwidth improvement," *IEEE Antennas Wireless Propag. Lett.*, vol. 22, pp. 1069–1073, 2023.

[7] S. A. Ali, M. Wajid, A. Kumar, and M. S. Alam, "Design challenges and possible solutions for 5G SIW MIMO and phased array antennas: A review," *IEEE Access*, vol. 10, pp. 88567–88594, 2022.

[8] W. D. Gu and Y. Zhang, "A type of dual/circularly polarized filtering dipole antenna design based on coupled lines," *IEEE Antennas Wireless Propag. Lett.*, vol. 24, pp. 489–493, 2025.

[9] Y.-W. Hsu, T.-C. Huang, H.-S. Lin, and Y.-C. Lin, "Dual-polarized quasi Yagi–Uda antennas with endfire radiation for millimeter-wave MIMO terminals," *IEEE Trans. Antennas Propag.*, vol. 65, no. 12, pp. 6282–6289, Dec. 2017.

[10] A. E. Farahat and K. F. A. Hussein, "28/38 GHz dual-band Yagi–Uda antenna with corrugated radiator and enhanced reflectors for 5G MIMO antenna systems," *Prog. In Electromagn. Res. C*, vol. 101, pp. 159–172, Jun. 2020.

[11] O. M. Haraz, M. Abdel-Rahman, N. Al-Khalli, S. Alshebeili, and A. R. Sebak, "Performance investigations of quasi-yagi loop and dipole antennas on silicon substrate for 94 GHz applications," *Int. J. Antennas Propag.*, vol. 2014, Jul. 2014, Art. no. 105625.

[12] L. Y. Feng, J. N. Hao, H. K. Zhao, W. S. Ji, and Y. Liu, "Design of singly fed dual-band antenna with a large frequency ratio by introducing a monopole mode to Yagi–Uda antenna," *IEEE Trans. Antennas Propag.*, vol. 71, no. 11, pp. 9042–9047, Nov. 2023.

[13] S. R. Isa, M. Jusoh, T. Sabapathy, M. R. Kamarudin, M. N. Osman, and A. Alomainy, "Multi-mode Yagi uda patch array antenna with non-linear inter-parasitic element spacing," *IEEE Access*, vol. 11, pp. 16346–16352, 2023.

[14] T. Zhao, Y. Xiong, X. Yu, H. Chen, M. He, L. Ji, X. Zhang, X. Zhao, H. Yue, and F. Hu, "A broadband planar quasi-yagi antenna with a modified bow-tie driverfor multi-band 3G/4G applications," *Prog. Electromagn. Res. C*, vol. 71, pp. 59–67, 2017.

[15] Q. Lou, R.-X. Wu, and Y. Tian, "A rectangular loop Yagi–Uda antenna by the two materials 3D printing technology," *IEEE Antennas Wireless Propag. Lett.*, vol. 17, pp. 2017–2020, 2018.

[16] L. P. Smith, J. C. Howell, and S. Lim, "A size-reduced, 15-element, planar Yagi antenna," *IEEE Trans. Antennas Propag.*, vol. 69, no. 4, pp. 2410–2415, Apr. 2021.
[17] C. Deng, W. Yu, and K. Sarabandi, "A compact vertically polarized fully metallic quasi-yagi antenna with high endfire gain," *IEEE Trans. Antennas Propag.*, vol. 70, no. 7, pp. 5959–5964, Jul. 2022.
[18] M. Nasir, A. Iftikhar, S. M. Abbas, R. Saleem, M. F. Shafique, and M. Alathbah, "A wideband broadside coupled Yagi antenna and arrays system for Ku band applications," *IEEE Access*, vol. 11, pp. 126967–126978, 2023.
[19] S. Kim and J. Choi, "Quasi-yagi slotted array antenna with fan-beam characteristics for 28 GHz 5G mobile terminals," *Appl. Sci.*, vol. 10, no. 21, p. 7686, Oct. 2020.
[20] L. Li, C. Zhang, Y. Shao, J. Yin, and J. Luo, "A SIW-fed double-helix antenna with broadband circular polarization for MMW applications," *IEEE Antennas Wireless Propag. Lett.*, vol. 21, pp. 361–365, 2022.
[21] H. Zahra, W. A. Awan, N. Hussain, S. M. Abbas, and S. Mukhopadhyay, "Helix inspired 28 GHz broadband antenna with end-fire radiation pattern," *Comput., Mater. Continua*, vol. 70, no. 1, pp. 1935–1944, 2022.
[22] A. Azari, A. Skrivervik, H. Aliakbarian, and R. A. Sadeghzadeh, "A super wideband dual-polarized Vivaldi antenna for 5G mmWave applications," *IEEE Access*, vol. 11, pp. 80761–80768, 2023.
[23] L. Zhou, M. Tang, J. Qian, Y.-P. Zhang, and J. Mao, "Vivaldi antenna array with heat dissipation enhancement for millimeter-wave applications," *IEEE Trans. Antennas Propag.*, vol. 70, no. 1, pp. 288–295, Jan. 2022.
[24] Q.-D. Cao, X.-X. Yang, F. Yu, and S. Gao, "High scanning rate millimeter-wave circularly polarized CTS leaky wave antenna," *IEEE Trans. Antennas Propag.*, vol. 72, no. 7, pp. 6087–6092, Jul. 2024.
[25] P. Sah and I. Mahbub, "A 38° wide beam-steerable compact and highly efficient V-band leaky wave antenna with surface integrated waveguide for vehicle-to-vehicle communication," in *Proc. IEEE Texas Symp. Wireless Microw. Circuits Syst. (WMCS)*, Apr. 2023, pp. 1–5.
[26] M. Nasir, Y. Xia, M. Jiang, and Q. Zhu, "A novel integrated Yagi–Uda and dielectric rod antenna with low sidelobe level," *IEEE Trans. Antennas Propag.*, vol. 67, no. 4, pp. 2751–2756, Apr. 2019.
[27] Y. Luo and Z. N. Chen, "Compressed dipoles resonating at higher order modes with enhanced directivity," *IEEE Trans. Antennas Propag.*, vol. 65, no. 11, pp. 5697–5701, Nov. 2017.
[28] Y. Luo, N. Zhang, Z. N. Chen, W. An, and K. Ma, "Synthesis of continuous source current for gain enhancement and sidelobe suppression of high-order mode dipoles," *IEEE Trans. Antennas Propag.*, vol. 71, no. 1, pp. 1047–1052, Jan. 2023.
[29] B. A. F. Esmail, S. Koziel, A. Pietrenko-Dabrowska, and D. Isleifson, "Wideband high-gain low-profile series-fed antenna integrated with optimized metamaterials for 5G millimeter wave applications," *Sci. Rep.*, vol. 14, no. 1, p. 185, Jan. 2024.
[30] M. Moniruzzaman, M. Mobarak, A. Alqahtani, T. Rahman, M. T. Islam, and M. Samsuzzaman, "Symmetrically structured epsilon negative metamaterial for antenna gain enhancement," *Opt. Mater.*, vol. 148, Feb. 2024, Art. no. 114777.
[31] Z. Wani, M. P. Abegaonkar, and S. K. Koul, "High-low-epsilon biaxial anisotropic lens for enhanced gain and aperture efficiency of a linearly polarized antenna," *IEEE Trans. Antennas Propag.*, vol. 68, no. 12, pp. 8133–8138, Dec. 2020.
[32] C. H. S. Nkimbeng, H. Wang, G. Byun, Y. B. Park, and I. Park, "Non-uniform metasurface-integrated circularly polarized end-fire dipole array antenna," *J. Electromagn. Eng. Sci.*, vol. 23, no. 2, pp. 109–121, Mar. 2023.
[33] C. M. Saleh, E. Almajali, A. Jarndal, J. Yousaf, S. S. Alja'Afreh, and R. E. Amaya, "Wideband 5G antenna gain enhancement using a compact single-layer millimeter wave metamaterial lens," *IEEE Access*, vol. 11, pp. 14928–14942, 2023.
[34] M. J. Jeong, N. Hussain, J. W. Park, S. G. Park, S. Y. Rhee, and N. Kim, "Millimeter-wave microstrip patch antenna using vertically coupled split ring metaplate for gain enhancement," *Microw. Opt. Technol. Lett.*, vol. 61, no. 10, pp. 2360–2365, Oct. 2019.
[35] D. Choi, M. A. Sufian, J. Lee, W. A. Awan, Y. Choi, and N. Kim, "Advanced metamaterial-integrated dipole array antenna for enhanced gain in 5G millimeter-wave bands," *Appl. Sci.*, vol. 14, no. 19, p. 9138, Oct. 2024.
[36] S. Koziel and A. Pietrenko-Dabrowska, "Reliable EM-driven size reduction of antenna structures by means of adaptive penalty factors," *IEEE Trans. Antennas Propag.*, vol. 70, no. 2, pp. 1389–1401, Feb. 2022.
[37] A. R. Conn, N. I. Gould, and P. L. Toint, "Trust region methods, MPS-SIAM series on optimization," Soc. Ind. Appl. Math., Philadelphia, PA, USA, Tech. Rep., 2000.
[38] H. Levy and F. Lessman, *Finite Diference Equations*. New York, NY, USA: Dover, 1992.
[39] *MATLAB Version*, MathWorks, Natick, MA, USA, 2021.

BASHAR A. F. ESMAIL (Member, IEEE) received the B.Eng. degree (Hons.) in electrical engineering (telecommunications) from Ibb University, Yemen, in 2008, and the M.Eng. and Ph.D. degrees in electrical engineering from the Universiti Tun Hussein Onn Malaysia, Malaysia, in 2017 and 2021, respectively. In 2021, he joined the Engineering Optimization and Modeling Center (EOMC), Department of Electrical Engineering, Reykjavík University, Iceland, as a Postdoctoral fellow. He is currently a Postdoctoral Researcher with the Department of Electrical and Computer Engineering, University of Manitoba, Canada. His research interests include the design and optimization of metamaterial structures, millimeter-wave antennas, MIMO systems, and reflector antennas for wireless and space applications.

DUSTIN ISLEIFSON (Senior Member, IEEE) received the Ph.D. degree in electrical and computer engineering from the University of Manitoba, Winnipeg, MB, Canada, in 2011. From 2013 to 2016, he was an Electrical Engineer with Magellan Aerospace, Winnipeg, where he worked on the Radarsat Constellation Mission (RCM). He has been with the Department of Electrical and Computer Engineering and the Centre for Earth Observation Science (CEOS), University of Manitoba, as an Assistant Professor, in 2016, and an Associate Professor, in 2022. His research interests include remote sensing, Arctic science, antenna design, and satellite technologies. He is the Chapter Chair of Winnipeg Section of IEEE GRS/AES.

SLAWOMIR KOZIEL (Fellow, IEEE) received the M.Sc. and Ph.D. degrees in electronic engineering from Gdańsk University of Technology, Poland, in 1995 and 2000, respectively, and the dual M.Sc. degrees in theoretical physics and in mathematics and the Ph.D. degree in mathematics from the University of Gdańsk, Poland, in 2000, 2002, and 2003, respectively. He is currently a Professor with the Department of Engineering, Reykjavík University, Iceland. His research interests include CAD and modeling of microwave and antenna structures, simulation-driven design, surrogate-based optimization, space mapping, circuit theory, analog signal processing, evolutionary computation, and numerical analysis.

ANNA PIETRENKO-DABROWSKA (Senior Member, IEEE) received the M.Sc. and Ph.D. degrees in electronic engineering from Gdańsk University of Technology, Poland, in 1998 and 2007, respectively. Currently, she is an Associate Professor with Gdańsk University of Technology. Her research interests include simulation-driven design, design optimization, control theory, modeling of microwave and antenna structures, and numerical analysis.